BOLLETTINO DI GEOFISICA TEORICA ED APPLICATA VOL. XXXIV, N. 133 - MARCH 1992

S. K. NATH [1], S. MAJUMDAR [2] and S. SENGUPTA [1]

TWO DIMENSIONAL SEISMIC MODELLING BY FINITE ELEMENT LEGENDRE POLYNOMIAL CONDENSATION TECHNIQUE

Abstract. A two dimensional forward modelling algorithm allowing anisotropy in density and wave propagation velocity for any geological model solves the wave equation by using the Finite Element Method. The condensation of global matrices is achieved by introducing hierarchical modes in the form of Legendre Polynomials. This does not only reduce the memory requirements and overall computational time to a great extent but also enables one to develope algorithms which are suitable for either multiple processors or mini-computers. The algorithm was successfully applied to simulate both the normal incidence and shot profile seismograms on several geological models by using an expansion of ten polynomials. Usually the harmonic modes associated with the deformation being simple, the simulation could have been done by using lower order polynomials. But the real earth models possess more complex modes and hence an allowance for higher order polynomials is kept in the program. A convergence test is also carried out both in space and time. The results presented in this paper indicate the efficiency and accuracy achieved by this method and its feasibility in computing synthetic seismograms for complex geological structures.

INTRODUCTION

Computation of synthetic seismograms involves generating amplitudes of seismic waves with travel times while propagating through a subsurface reflectivity model associated with a specified velocity-depth model.

Seismic modelling dates back almost six decades as different authors examined variations in seismic wave amplitude with depth and the effects of buried structures viz. faults, folds, channels etc. The analytical modelling techniques based on the Kirchoff Integral (Hilterman, 1970), Finite Difference (Kelly et. al., 1976), Fourier method (Gazdag, 1981; Kosloff and Baysal, 1982), F-K Domain Solution to the Wave Equation (Sherwood et al., 1983), Frequency and Space Domain Modelling (Kelamis and Kjartansson, 1985; Choate, 1982), Elastic Forward Modelling (Reshef et. al, 1988), and Time Series Approach (Robinson and Treitel, 1966, 1977) need special mention.

Recent developments in the finite element method instilled an expectation in the minds of exploration geophysicists that any geological model can be properly simulated on a digital computer. Many attempts were made in this regard. The effects on surface waves as they propagate through irregular structures had been studied by Drake (1972) using an eigenvalue approach. For seismic body waves, Bolt and Smith (1976) demonstrated that finite elements can be used to compute the response of irregular structures in the time domain. Potentially accurate direct methods were developed by Drake and Asten (1982) and Marfurt (1984). Asten,

Manuscript received October 1, 1990; accepted March 5, 1992.

[1] Department of Geology and Geophysics, Indian Institute of Technology, Kharagpur 721302, India.

[2] Department of Civil Engineering, Indian Institute of Technology, Kharagpur 721302, India.

et al. (1984) could even successfully model in-seam Love Wave scattering by the finite element method.

The direct finite element modelling scheme needs the efficient networking of computers with large memory, disk storage, faster CPUs and parallel processors for computing and storing enormous volume of data. Also the computational time is extremely high. However, this is no reason to lag behind in the search of more economical and efficient algorithms. The present work is developed with two objectives in mind - (i) reduction of memory requirements and (ii) development of an algorithm which will be suitable for multiple processors on the one hand and mini-computers on the other.

In the present work, an intermediate procedure of condensation of the global matrices by using hierarchical modes in the form of Legendre Polynomials (Majumdar and Samanta, 1988) is introduced. Previously, the condensation of the global matrices was achieved by introducing harmonic expansion in Fourier Series (Nath, et al., 1990, 1991).

The Legendre Polynomial Condensation enables one not only to design a CPU bound algorithm but also to successfully model any buried geological structure in a greatly reduced time.

In this paper, the results of a convergence test both in space and time, a simulated split-spread shot profile and the synthetic normal incidence seismograms for a few geological models are presented to establish the accuracy and efficiency of the condensation modelling technique.

BASIC THEORY

A general review of the Finite Element Method can be found in Desai and Abel (1972), Cook (1974), Bathe and Wilson (1976) and Zienkiewicz (1977).

The basic Wave Equation for the displacement vector $\underline{U}(t)$ can be written in the matrix form as

$$\underline{M}\,\ddot{\underline{U}}(t)+\underline{C}\,\dot{\underline{U}}(t)+\underline{K}\,\underline{U}(t)=\underline{F}(t), \tag{1}$$

where

$\underline{M}$ = the global mass matrix,

$\underline{K}$ = the global stiffness matrix,

$\underline{C}$ = the global damping matrix,

$\ddot{\underline{U}}(t)$ = the acceleration vector $\dfrac{d^2\underline{U}}{dt^2}$,

$\dot{\underline{U}}(t)$ = the particle velocity vector $\dfrac{d\underline{U}}{dt}$

$\underline{U}(t)$ = the displacement vector,

$\underline{F}(t)$ = the array of global external dynamic force vectors.

Fig. 1 represents the complete geometry of the Finite Element Simulation including the isoparametric mapping of the global model, condensation, meshing etc.

Isoparametric mapping and discretization

Fig. 1a represents a global model subdivided into four macro-structures depending on the anisotropy in the density and velocity pairs. The origin is located at the centroid of the global model. The primary nodes with known co-ordinates are numbered as shown in Fig. 1a.

The discretization of each macro-structure starts with the isoparametric mapping of the individual structure of the global xy space into a local $\xi\eta$ space and mapping each element back into the global domain. This is illustrated in Figs. 1b and 1c. Fig. 1b represents the macro-structure I of the global model in the xy space. The primary global nodes 5, 4, 1 and 2 re-

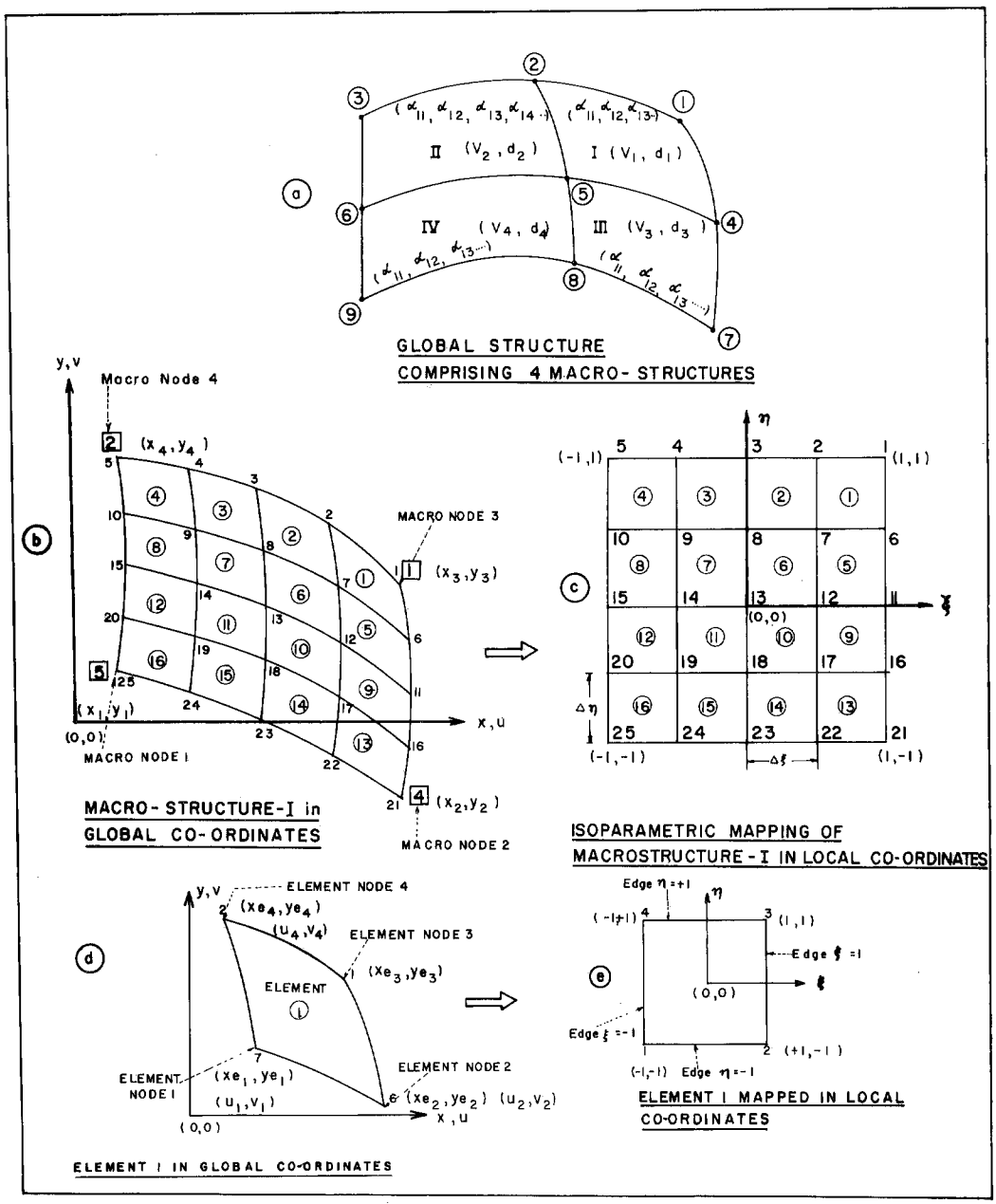

Fig. 1 - Finite Element discretization, isoparametric mapping and condensation.

present the macronodes 1, 2, 3 and 4 respectively, with the co-ordinates (x_1, y_1), (x_2, y_2), (x_3, y_3) and (x_4, y_4) respectively. The right hand rule is strictly followed in numbering the nodes. This macro-structure is mapped into a square structure in the local $\xi\eta$ space with the co-ordinates (–1, –1), (1, –1), (1, 1), (–1, 1) corresponding to the global co-ordinates (x_1, y_1), (x_2, y_2), (x_3, y_3) and (x_4, y_4) respectively. Depending on the fineness required for the simulation, the structure is subdivided into a number of elements in the $\xi\eta$ space as shown in Fig. 1c. The nodes are numbered and the local $\xi\eta$ co-ordinates at each node are computed with respect to the master nodes. All elements in the local space are then mapped back into the xy space. For example, element 1 in the local space bounded by the nodes 7, 6, 1 and

2 will have the following $\xi\eta$ co-ordinates:

$$\begin{aligned}
&\textit{Node 7: } (\xi_1 = 1-\Delta\xi)\\
&\qquad\quad (\eta_1 = 1-\Delta\eta),\\
&\textit{Node 6: } (\xi_2 = 1)\\
&\qquad\quad (\eta_2 = 1-\Delta\eta),\\
&\textit{Node 1: } (\xi_3 = 1)\\
&\qquad\quad (\eta_3 = 1),\\
&\textit{Node 2: } (\xi_4 = 1-\Delta\xi)\\
&\qquad\quad (\eta_4 = 1).
\end{aligned}$$

Element 1 when mapped back into the global space, as shown in Fig. 1b and represented megascopically in Fig. 1d, will have the global co-ordinates (xe_1, ye_1), (xe_2, ye_2), (xe_3, ye_3) and (xe_4, ye_4) for the nodes 7, 6, 1 and 2 respectively. With the help of individual shape functions N_1, N_2, N_3 and N_4, the corner co-ordinates can be computed as follows:

$$xe_i = N_{1|(\xi_i, \eta_i)} x_1 + N_{2|(\xi_i, \eta_i)} x_2 + N_{3|(\xi_i, \eta_i)} x_3 + N_{4|(\xi_i, \eta_i)} x_4, \tag{2}$$

$$ye_i = N_{1|(\xi_i, \eta_i)} y_1 + N_{2|(\xi_i, \eta_i)} y_2 + N_{3|(\xi_i, \eta_i)} y_3 + N_{4|(\xi_i, \eta_i)} y_4, \tag{3}$$

where,

$$N_{1|(\xi_i, \eta_i)} = 0.25\ (1-\xi_i)\ (1-\eta_i), \tag{4}$$

$$N_{2|(\xi_i, \eta_i)} = 0.25\ (1+\xi_i)\ (1-\eta_i), \tag{5}$$

$$N_{3|(\xi_i, \eta_i)} = 0.25\ (1+\xi_i)\ (1+\eta_i), \tag{6}$$

$$N_{4|(\xi_i, \eta_i)} = 0.25\ (1-\xi_i)\ (1+\eta_i). \tag{7}$$

As highlighted in Fig. 1d, the nodes 7, 6, 1 and 2 bounding the element 1 actually represent the element nodes 1, 2, 3 and 4 respectively. The *x*-parallel and *y*-parallel components of the displacement vectors at the nodes 1, 2, 3 and 4 are (u_1, v_1), (u_2, v_2), (u_3, v_3) and (u_4, v_4), respectively.

Once the corner co-ordinates in the *xy* space are calculated by forward and backward mapping, each four-node element is finally mapped into an isoparametric square element as shown in Fig. 1e for the computation of the element local stiffness and mass matrices.

Element stiffness and mass matrices

The basic expressions for the element stiffness and mass matrices are as follows:

$$\underline{k}_e = \int \int \underline{B}^T \underline{D}\ \underline{B}\ h\ dx\ dy, \tag{8}$$

$$\underline{m}_e = \varrho \int \int \underline{N}^T \underline{N}\ dx\ dy. \tag{9}$$

In the above expressions,

$\underline{k}_e$ = the element stiffness matrix,

$\underline{m}_e$ = the element mass matrix,

h = the thickness of the element,

ϱ = the material density of the element,

$\underline{B}$ = the Strain-Displacement Matrix of the element,

$\underline{D}$ = the Constitutive Matrix of the element,

$\underline{N}$ = the Shape Function Matrix of the element.

Using the isoparametric formulation, the above two expressions can be written in the summation form in the local co-ordinates as

$$\underline{k}_e = \sum_{i=1}^{ng} \sum_{j=1}^{ng} \underline{B}^T \underline{D}\, \underline{B}\, h|\underline{j}|\, W_i W_j, \tag{10}$$

$$\underline{m}_e = \sum_{i=1}^{ng} \sum_{j=1}^{ng} \varrho\, \underline{N}^T \underline{N}\, |\underline{j}|\, W_i\, W_j, \tag{11}$$

where ng is the number of Gauss points in the element, W_i and W_j are the weighting functions at those Gauss points and $\underline{j}$ is the Jacobian matrix.

The element being isoparametric, considering Figs. 1d and 1e, we can write the global co-ordinates and displacements in terms of the corner co-ordinates, nodal degrees of freedom and individual shape functions as

$$x = \sum_{i=1}^{4} N_i\, xe_i, \tag{12}$$

$$y = \sum_{i=1}^{4} N_i\, ye_i, \tag{13}$$

$$u = \sum_{i=1}^{4} N_i\, u_i, \tag{14}$$

$$v = \sum_{i=1}^{4} N_i\, v_i, \tag{15}$$

where u_i and v_i are the x-parallel and y-parallel components of the displacement vectors at respective nodes. Eqns. (14) and (15) can be together put in terms of the nodal degrees of freedom $\{\underline{d}\}$ and the shape fuction matrix $\underline{N}$ as follows:

$$\{u\ v\} = \underline{N}\ \{\underline{d}\}, \tag{16}$$

and

$$\{\underline{d}\} = \{u_1\ u_2\ u_3\ u_4\ v_1\ v_2\ v_3\ v_4\}. \tag{17}$$

The shape function matrix $\underline{N}$ can therefore be written in terms of the individual shape functions as

$$\underline{N}=\begin{bmatrix} N_1 & N_2 & N_3 & N_4 & 0 & 0 & 0 & 0 \\ 0 & 0 & 0 & 0 & N_1 & N_2 & N_3 & N_4 \end{bmatrix}. \tag{18}$$

The strain-displacement relation can be given as,

$$\{\epsilon\}=\underline{B}\,\underline{U}_o, \tag{19}$$

where

$$\underline{U}_o^{\mathrm{T}}=\{\underline{d}\}, \tag{20}$$

and $\{\epsilon\}$ is the strain vector.

By considering the x-parallel displacement u and invoking the co-ordinate transformation of the derivatives, the following expression can be obtained:

$$\begin{Bmatrix} \frac{\partial u}{\partial x} \\ \frac{\partial u}{\partial y} \end{Bmatrix} = \begin{bmatrix} \frac{\partial \xi}{\partial x} & \frac{\partial \eta}{\partial x} \\ \frac{\partial \xi}{\partial y} & \frac{\partial \eta}{\partial y} \end{bmatrix} \begin{Bmatrix} \frac{\partial u}{\partial \xi} \\ \frac{\partial u}{\partial \eta} \end{Bmatrix}, \tag{21}$$

or

$$\begin{Bmatrix} \frac{\partial u}{\partial x} \\ \frac{\partial u}{\partial y} \end{Bmatrix} = \underline{j}^{-1} \begin{Bmatrix} \frac{\partial u}{\partial \xi} \\ \frac{\partial u}{\partial \eta} \end{Bmatrix}. \tag{21a}$$

The above transformation is also true for the y-parallel component v.

The Jacobian matrix $\underline{j}$ can be written as

$$\underline{j}=\begin{bmatrix} \frac{\partial x}{\partial \xi} & \frac{\partial y}{\partial \xi} \\ \frac{\partial x}{\partial \eta} & \frac{\partial y}{\partial \eta} \end{bmatrix}. \tag{22}$$

The strain vector $\{\epsilon\}$ can also be defined as

$$\{\epsilon\}=\underline{H}\begin{Bmatrix} u_{,x} \\ u_{,y} \\ v_{,x} \\ v_{,y} \end{Bmatrix}, \tag{23}$$

where $\underline{H}$ is a constant matrix and can be represented as

$$\underline{H}=\begin{bmatrix} 1 & 0 & 0 & 0 \\ 0 & 0 & 0 & 1 \\ 0 & 1 & 1 & 0 \end{bmatrix}, \tag{24}$$

Again,

$$\begin{Bmatrix} u,_x \\ u,_y \\ v,_x \\ v,_y \end{Bmatrix} = \underline{J}^{-1} \begin{Bmatrix} u,_\xi \\ u,_\eta \\ v,_\xi \\ v,_\eta \end{Bmatrix} , \tag{25}$$

where

$$\underline{J}^{-1} = \begin{bmatrix} [j]^{-1} & [0] \\ [0] & [j]^{-1} \end{bmatrix} . \tag{26}$$

Using the eqn. (14) and invoking the derivative with respect to ξ and η, we can write

$$\begin{Bmatrix} u,_\xi \\ u,_\eta \end{Bmatrix} = \begin{bmatrix} N_{1,\xi} & N_{2,\xi} & N_{3,\xi} & N_{4,\xi} \\ N_{1,\eta} & N_{2,\eta} & N_{3,\eta} & N_{4,\eta} \end{bmatrix} \begin{Bmatrix} u_1 \\ u_2 \\ u_3 \\ u_4 \end{Bmatrix} . \tag{27}$$

If we define

$$\begin{bmatrix} N_{1,\xi} & N_{2,\xi} & N_{3,\xi} & N_{4,\xi} \\ N_{1,\eta} & N_{2,\eta} & N_{3,\eta} & N_{4,\eta} \end{bmatrix} = [b], \tag{28}$$

then

$$\begin{Bmatrix} u,_\xi \\ u,_\eta \\ v,_\xi \\ v,_\eta \end{Bmatrix} = \begin{bmatrix} [b] & [0] \\ [0] & [b] \end{bmatrix} \underline{U}_n \tag{29}$$

if we further define

$$\underline{B}_n = \begin{bmatrix} [b] & [0] \\ [0] & [b] \end{bmatrix} . \tag{30}$$

Using the eqn. (23), (25) and (29), the strain vector $\{\epsilon\}$ can be redefined as

$$\{\epsilon\} = \underline{H}\, \underline{J}^{-1}\, \underline{B}_n\, \underline{U}_n . \tag{31}$$

Finally, comparing the eqn. (19) and (31), the strain-displacement matrix $\underline{B}$ can be written as

$$\underline{B} = \underline{H}\, \underline{J}^{-1}\, \underline{B}_n . \tag{32}$$

Condensation and time integration

The displacement vector $\underline{U}$ at any node given by eqn. (33) may be approximated by rolling independent Legendre Polynomials in the x and y directions. This approximation is possible

because like the trigonometric functions of Fourier Series, the Legendre Polynomials are also orthogonal functions. The Legendre Polynomial expansion of the components of $\underline{U}$ can be given by eqns. (34) and (35):

$$\underline{U}= \begin{Bmatrix} u \\ v \end{Bmatrix}, \tag{33}$$

$$u= \sum_{i=0}^{n} \sum_{j=0}^{m} \alpha_{ij} P_i(x) P_j(y), \tag{34}$$

$$v= \sum_{i=0}^{n} \sum_{j=0}^{m} \alpha_{(i+mn)(j+mn)} P_i(x) P_j(y), \tag{35}$$

where α is the global parameter matrix for the global structure as shown in Fig. 1a, and $P_i(x)$ and $P_j(y)$ are the associated Legendre Polynomials in the x and y directions respectively.

Eqns. (14) and (15) provide the isoparametric mapping of the displacement components necessary for FEM formulations of a four-noded element, whereas the eqns. (34) and (35) are the Fourier representation of the displacement components in terms of the parametric variables and the deformation harmonics.

Hence, the eqn. (33) may be represented in terms of the matrix $\underline{\alpha}$ as follows:

$$\underline{U}=\underline{T}\,\underline{\alpha}. \tag{36}$$

$\underline{T}$, the element condensation matrix, can be written as

$$\underline{T}= \begin{bmatrix} [t] & [0] \\ [0] & [t] \end{bmatrix}, \tag{37}$$

such that

$$[t]= \begin{bmatrix} P_0(xe_1)\,P_0(ye_1) & P_0(xe_1)\,P_1(ye_1) & \cdots\cdots \\ P_0(xe_2)\,P_0(ye_2) & P_0(xe_2)\,P_1(ye_2) & \cdots\cdots \\ P_0(xe_3)\,P_0(ye_3) & P_0(xe_3)\,P_1(ye_3) & \cdots\cdots \\ P_0(xe_4)\,P_0(ye_4) & P_0(xe_4)\,P_1(ye_4) & \cdots\cdots \end{bmatrix}. \tag{38}$$

The condensation matrix $\underline{T}$ transforms the element stiffness matrix $\underline{k}_e$ into $\underline{\hat{k}}_e$, element mass matrix $\underline{m}_e$ into $\underline{\hat{m}}_e$ and the array of external force vectors $\underline{f}_e$ into $\underline{\hat{f}}_e$ such that

$$\underline{\hat{k}}_e=\underline{T}^T\,\underline{k}_e\,\underline{T}, \tag{39}$$

$$\underline{\hat{m}}_e=\underline{T}^T\,\underline{m}_e\,\underline{T}, \tag{40}$$

$$\underline{\hat{f}}_e=\underline{T}^T\,\underline{f}_e \tag{41}$$

Since by condensation the degree of freedom is reduced, $\underline{T}^T$ will reduce the number of equations and at the same time will condense the local stiffness and mass matrices into the symmetric global matrices. $\underline{T}^T$ will transform the local force vector or the array of local force

vectors into an equivalent condensed global force vector or an array of force vectors.

The condensed stiffness, mass and the array of force vectors of the individual elements of the entire global structure are added together to assemble the corresponding global matrices $\underline{K}$, $\underline{M}$ and $\underline{F}$.

The dimension of $\underline{K}$ and $\underline{M}$ will be (pxp) such that

$p = 2$x (the no. of Legendre polynomials in the x direction) x the no. of Legendre polynomials in the y direction).

In the direct finite element method, the dimension p would have been equal to twice the number of total nodes in the structure. For example, if a structure is defined by 3000 nodes, the dimensions of the global matrices will be (6000x6000). But by Legendre Polynomial condensation, the dimension reduces to merely (50x50) if 5 polynomials are considered in both the x and y directions. Although in this technique few extra mathematical operations are involved, there are significant reductions in the overall computational time, memory requirements and disk storage. This also facilitates modelling on a mini-computer.

It is very difficult to assess the global damping matrix $\underline{C}$. Actually, it should be determined from the attenuation of the waves obtained from the field records. However, it is common practice to assume the $\underline{C}$ matrix to be proportional to the mass $\underline{M}$ and stiffness $\underline{K}$ matrices. For example, $\underline{C} = \beta\underline{M} + \gamma\underline{K}$, where β and γ are the proportionality constants.

The wave equation (1) thus gets transformed into the following form and is solved by the Cholesky Decomposition and Central Difference Method (Bathe and Wilson, 1976):

$$\underline{\alpha}_{|(t+\Delta t)}\left[\frac{\underline{M}}{\Delta t^2} + \frac{\underline{C}}{2\Delta t}\right] = \underline{F}(t) - \left[\underline{K} - \frac{2\underline{M}}{\Delta t^2}\right]\underline{\alpha}_{|(t)} - \left[\frac{\underline{M}}{\Delta t^2} - \frac{\underline{C}}{2\Delta t}\right]\underline{\alpha}_{|(t-\Delta t)}, \tag{42}$$

where Δt is the sampling interval and t is the instant of time at which the response is computed.

Since $\underline{U}$ is a function of $\underline{\alpha}$, $\underline{x}$ and $\underline{y}$ solving for $\underline{\alpha}$, $\underline{U}$ is calculated, which on differentiation by the central difference method gives the particle velocity vector and hence the seismic response at a particular node.

COMPUTATIONAL ALGORITHM

The source code is written in Fortran-77 and run on a Hewlett-Packard 9330 system. The computational algorithm can be summarised as follows:

Step 1: Automatic discretization of all the macrostructures of the model by isoparametric mapping.

Step 2: Computation of minimum dimensions of an element from the knowledge of least velocity, sampling rate and duration of the source pulse.

Step 3: Computation of local mass, local stiffness and condensation matrices for all the elements of each macrostructure.

Step 4: Check for the convergence of the matrices.

Step 5: Transformation of local matrices into the corresponding condensed matrices.

Step 6: Global assemblage of all the condensed local matrices.

Step 7: Formation of the array of local external force vectors for all the elements; their condensation; assembly into the global array and check for the duration of the pulse.

Step 8: Introduction of boundary conditions and compaction of the base of the model to make it a rigid and undeformable basement.

Step 9: Initialisation of the damping matrix.

Step 10: Cholesky Decomposition and Time Integration.

Step 11: Computation of final global displacement parameter vector.

Step 12: Computation of Displacement Vector.

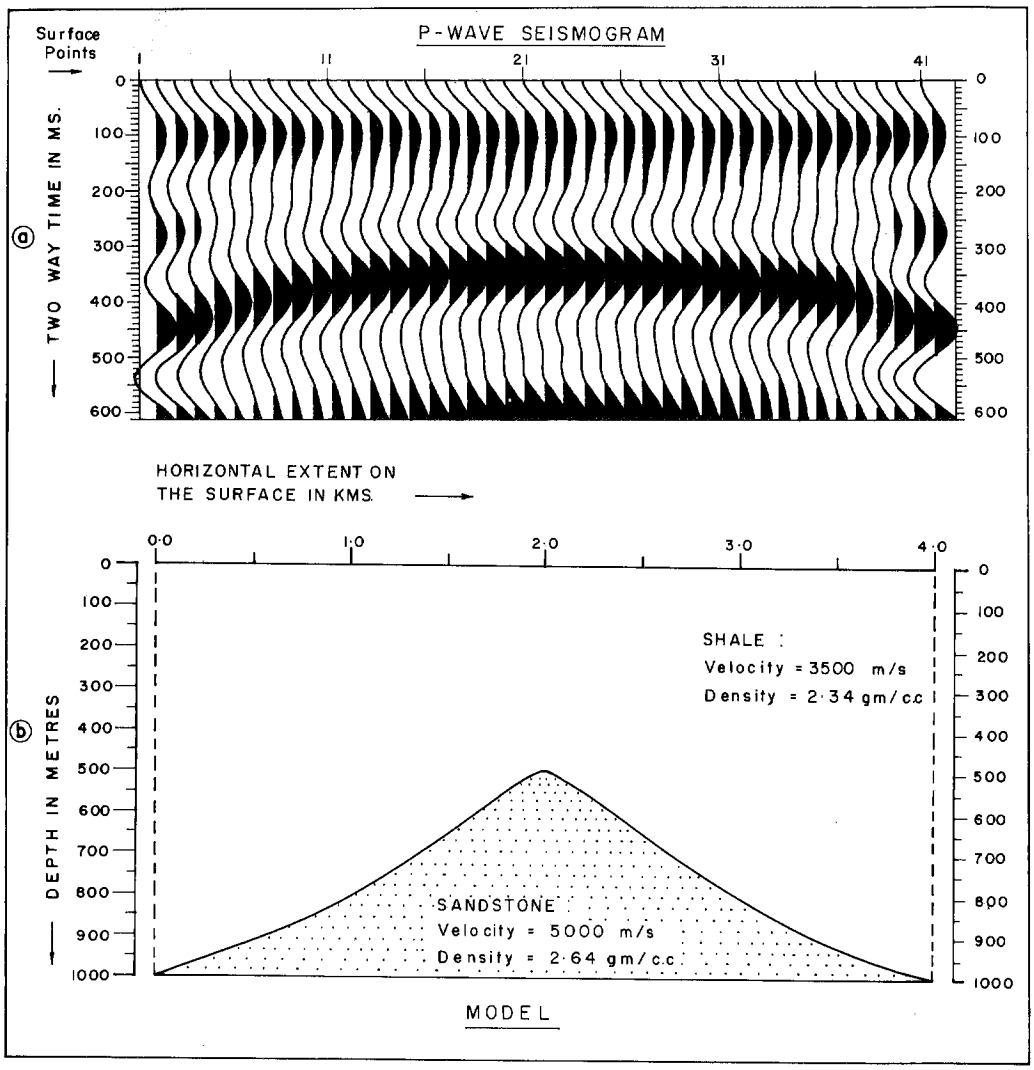

Fig. 2 - a) Normal Incidence Synthetic Time section for the deep-seated anticlinal structure simulated by 12,700 elements and 0.05 ms sample interval.
b) A deep-seated anticlinal model (4 km x 1 km); configuration and physical parameters.

Step 13: Differentiation to generate particle velocity vector.

Step 14: Demultiplexing.

Step 15: Storage and plotting.

MODEL STUDIES AND DISCUSSION

The following model studies are carried out using the numerical algorithm described in the earlier section. In all cases, ten Legendre Polynomials are used for condensation. Further, in each model, all the base elements are fixed but elements at the edge boundaries are free to move.

A deep-seated anticlinal model

Fig. 2b represents the physical configuration of an anticlinal model with the top compact

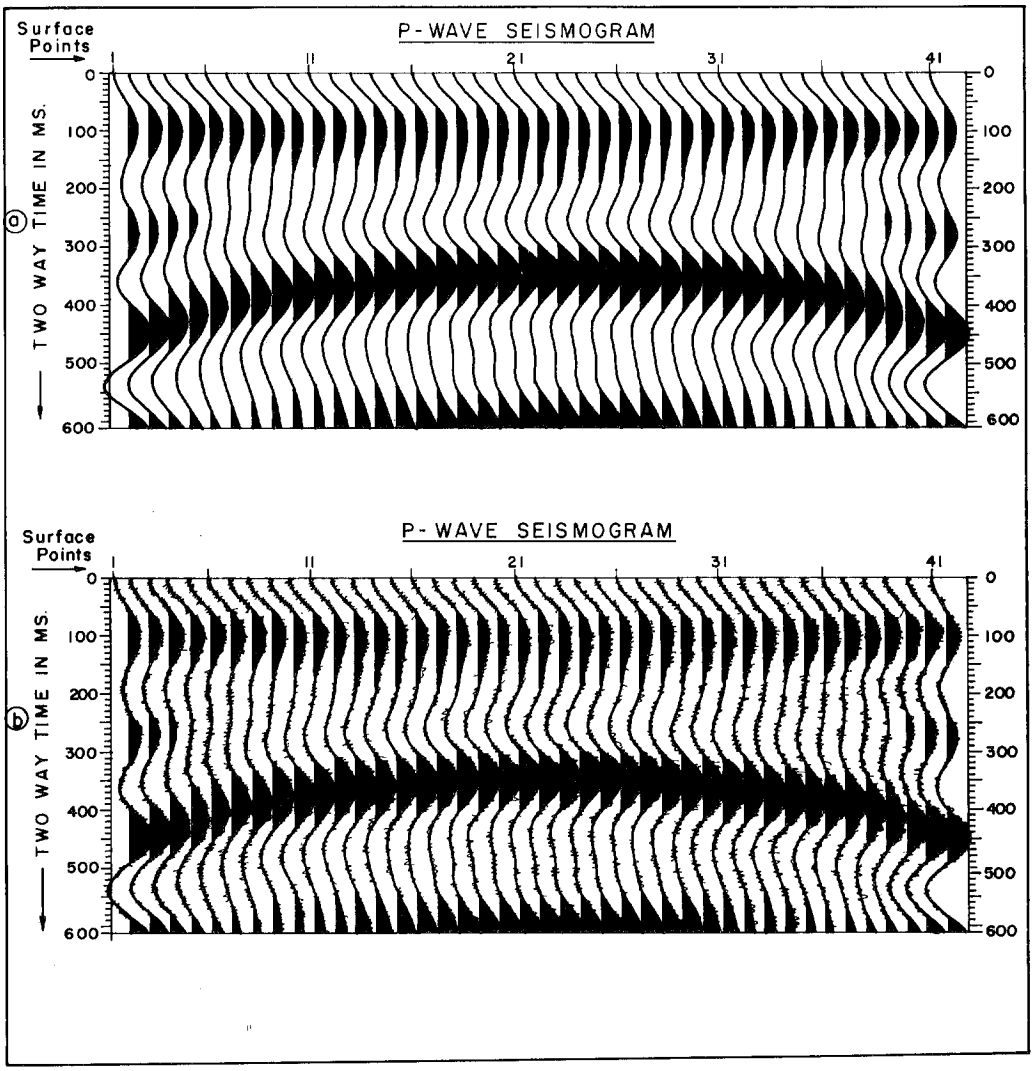

Fig. 3 - Normal Incidence Synthetic Time section for the deep-seated anticlinal structure of Fig. 2b simulated by a) 20,500 elements and 0.05 ms sample interval and b) 32,250 elements and 0.025 ms sample interval.

Table - Comparison of seismic responses (vertical component of particle velocities in m/s).
As simulated by the Finite Element Method (FEM) and Legendre Polynomial Condensation Method (LPCM) at surface positions 1 and 21 of Fig. 4 at different time steps. The sampling interval is 0.025 ms.

Time step	Seismic Responses Simulated By			
	F.E.M. at nodes		L.P.C.M. at nodes	
	1	21	1	21
1000	2.65209E-06	5.66548E-06	2.29575E-06	4.67021E-06
5000	-1.96775E-05	4.01578E-05	-1.67687E-05	3.59863E-05
10000	2.00013E-05	-1.66907E-05	1.73427E-05	-1.41615E-05

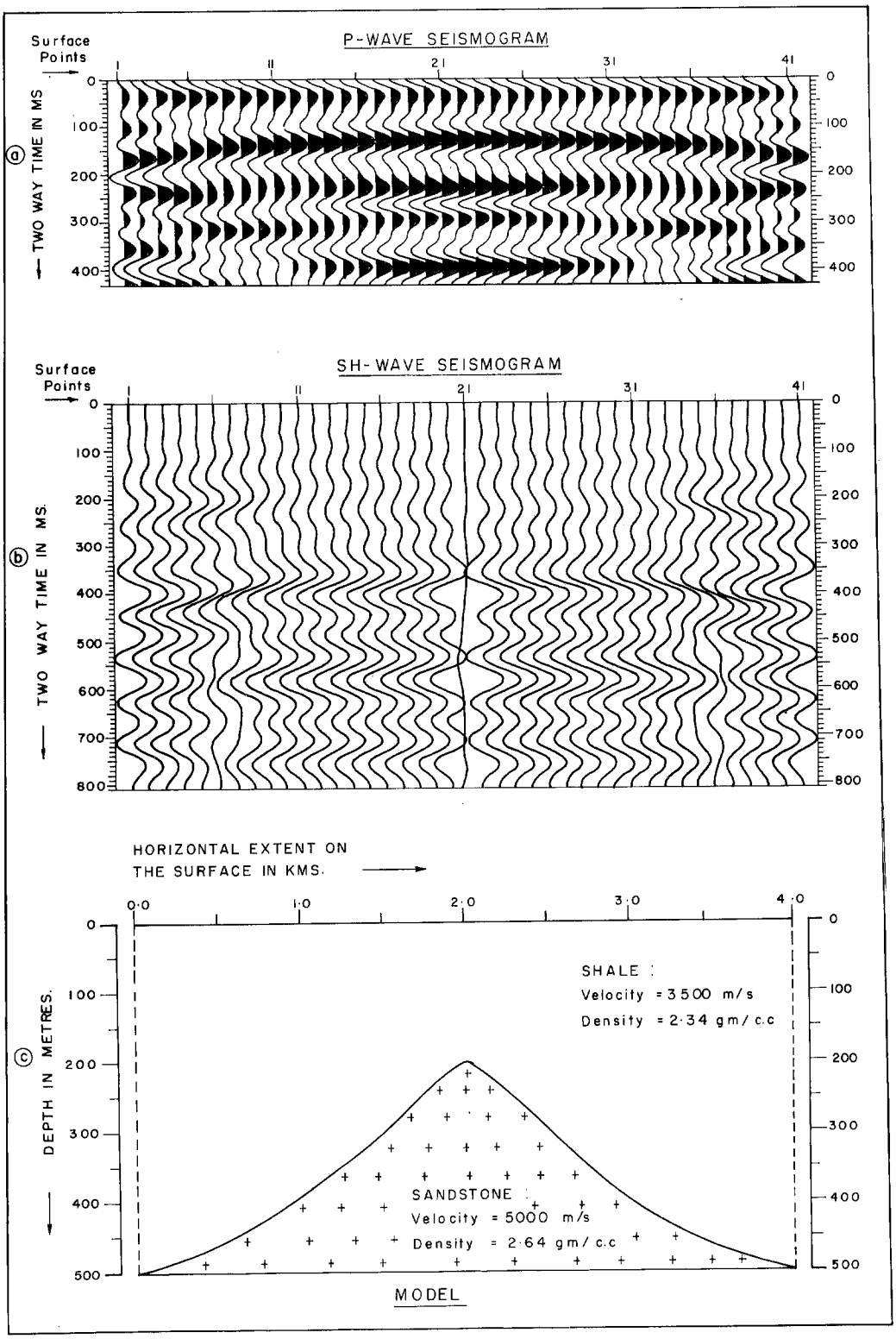

Fig. 4 - a) P-wave seismogram simulated by 12,700 elements and 0.025 ms sampling interval.
b) SH-wave seismogram simulated by 12,700 elements and 0.025 ms sampling interval.
c) A shallow anticlinal model (4 km x 0.5 km); configuration and physical parameters.

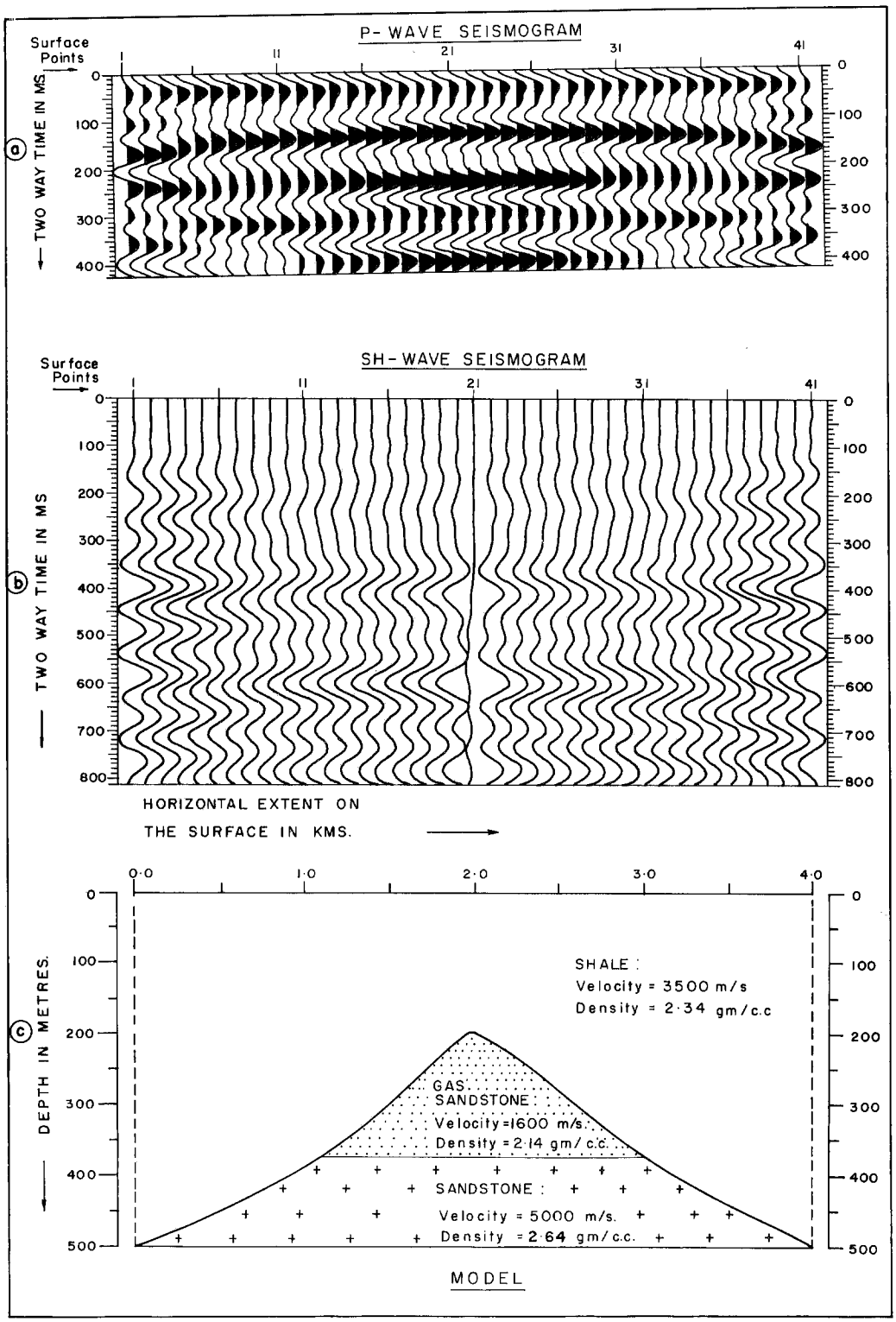

Fig. 5 - a) P-wave seismogram simulated by 13,500 elements and 0.025 ms sampling interval.
b) SH-wave seismogram simulated by 13,500 elements and 0.025 ms sampling interval.
c) An anticlinal model with an intermediate gas sandstone layer (4 km x 0.5 km); configuration and physical parameters.

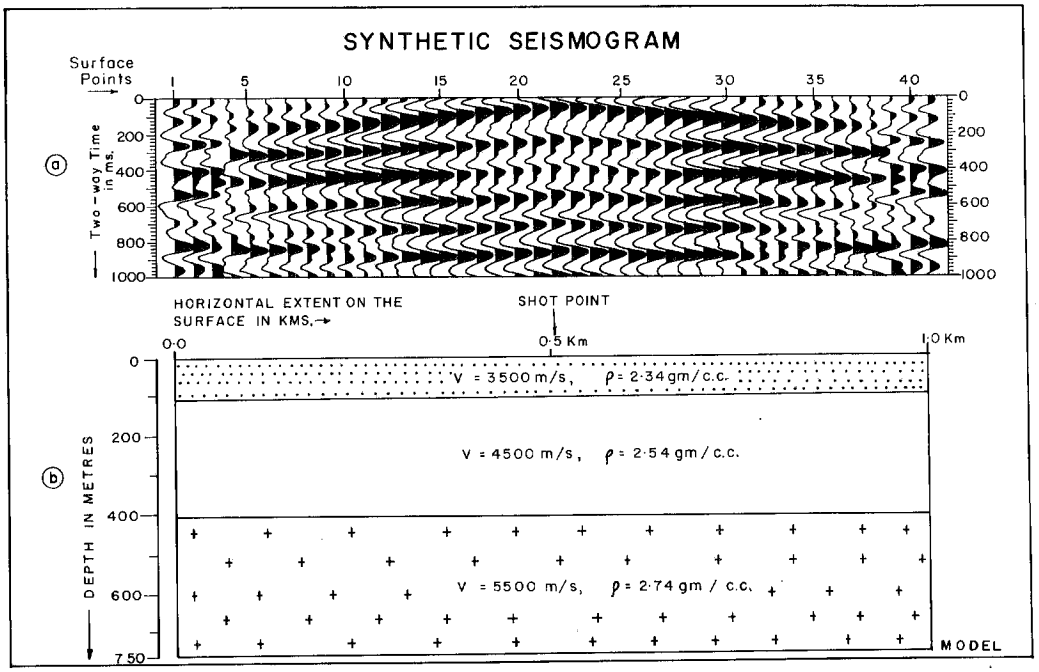

Fig. 6 - a) A synthetic 41 channel split - spread seismic record.
b) A three layered earth model; configuration and physical parameters.

shale layer having wave propagation velocity of 3500 m/s and density 2.34 gm/cc, and the bottom consolidated sandstone layer with wave propagation velocity of 5000 m/s and density 2.64 gm/cc. The entire model has a dimension of 4 km x 1 km in the x and y directions. The apex of the anticline is situated at a depth of 0.5 km from the surface. This model is discretized into 12,700 elements and normal incidence seismic responses are computed at 41 source-receiver locations on the surface with a trace interval of 100 m. The external vertical force applied is impulsive in nature with a duration of one sample interval and its amplitude is 10,000 Newtons. The modelling scheme is such that on application of the impulse at a position on the surface, the response is calculated only at that position for the entire time span. The source and receiver are then shifted to the next location and so forth. This simulates a NMO corrected CDP time section used in actual practice by exploration geophysicists. In Fig. 2(a), the simulated P-wave seismogram computed for 20,000 time steps at 0.05 ms sampling interval is presented in VAW mode. The strong and consistent reflection event between 300 ms and 500 ms represents the anticlinal surface. But the frequency content is comparatively lower, the dominant frequency being about 20 Hz.

A shallower anticlinal model

A model of a shallower anticline is shown in Fig. 4c. The density and velocity contrasts of the upper and lower layers are the same as the previous deep-seated anticlinal model of Fig. 2b; the only difference between these two models lies in their dimensions and the depth of the apexes. The anticlinal model of Fig. 4c has the dimensions of 4 km x 500 m in the x and y directions and the apex of the anticline is situated at a depth of 200 m from the surface. The entire model is discretized into 12,700 elements and normal incidence synthetic time sections comprising 41 traces at 100 m spacing are computed for a span of 40,000 time steps at 0.025 ms sampling interval. An impulsive external vertical force of 10,000 N amplitude and one sample duration is applied. In Fig. 4a, the P-wave seismogram is presented in VAW mode and SH-wave seismogram is shown in Fig. 4b in wiggle mode. The P-wave seismogram indicates a strong and consistent reflection event between 100 ms and 200 ms, whereas in

the SH-wave seismogram this event is received late, between 200 ms and 300 ms, as the S-wave propagation is comparatively slower than the P-wave propagation. The frequency content in this shallow event is much higher than that observed in the case of the deep-seated model of Fig. 2, the dominant frequency being about 60 Hz.

An anticlinal model with intermediate gas sandstone layer

Fig. 5c shows the physical configuration of an anticlinal model with a gas sandstone at the apex of the anticline. The upper shale has a wave propagation velocity of 3500 m/s and density 2.34 gm/cc. The intermediate gas sandstone concentrated only at the apex region has a velocity contrast of 1600 m/s and density contrast of 2.14 gm/cc, whereas the harder sandstone layer at the bottom has 5000 m/s as propagation velocity and 2.64 gm/cc as density. The dimension of the entire structure is 4 km x 500 m in *xy* space. The model is discretized into 13,500 elements and normal incidence seismic responses for 40,000 time steps at 0.025 ms sampling rate are calculated at 41 source-receiver locations at 100 m spacing on the surface. The external impulsive force applied is of the same strength and duration as that used in the previous simulations. The P-wave and SH-wave seismograms are presented in Figs. 5a and 5b in VAW and wiggle modes respectively. A feeble bright spot effect can be observed at around 360 ms in the P-wave seismogram.

Shot profile simulation

Fig. 6b represents a three layered earth model with flat interfaces. The top layer has a wave propagation velocity of 3500 m/s and density of 2.34 gm/cc. The velocity and density contrasts for the intermediate stratum are 4500 m/s and 2.54 gm/cc, respectively. In the base layer, the wave propagation velocity is 5500 m/s and the density is 2.74 gm/cc. The model dimension is 1 km x 750 m in the horizontal and depth directions. The thickness of the top layer is 100 m, that of the intermediate stratum is 300 m. The base layer is limited to 750 m depth and all the elements belonging to the base level are compacted as in all the previous cases. The entire model is discretized into 15,000 four-node elements. In order to simulate a split-spread shot record, the dynamic global force vector is formed by applying an external force of 10,000 N only at the mid surface position 21. The source pulse is allowed to act upon the system for a duration of one sample only. For the impulse at location 21, the seismic responses are computed at all 41 receiver positions on the surface at 25 m channel interval including the one at 21. The time integration is performed at 0.025 ms time step. The simulated 41 channel split-spread record is displayed in Fig. 6a in VAW mode. The reflection hyperbolas are clearly visible in the record. The reflection events are symmetric with respect to those at position 21. The seismic event at 50 ms to 150 ms between traces 21-4 and 21-38 indicates the primary reflections from the upper interface at the 100 m depth level. Its multiple effect is observed at 300 ms to 450 ms between traces 21-4 and 21-38. The seismic pattern at 200 ms to 300 ms between traces 21-4 and 21-38 represents the primary reflections from the second interface at the 400 m depth level. Its multiple is seen at 550 ms to 600 ms between traces 21-4 and 21-38. Traces 1-3 and 39-41 show noisy responses due to the intermingling of the reflection signals with side scattering.

Convergence in space and time

A qualitative convergence test is carried out in both space and time. The objective of this test is to prove that by either slightly increasing the fineness in meshing or reducing the sampling inverval or both, the characteristic pattern of the simulated seismic responses remains unchanged. The meshing is usually done from the knowledge of the least velocity of wave propagation in a medium, the duration of the source pulse and the sampling interval.

In order to establish the above, the physical model of Fig. 2b is considered. In Fig. 2a, as discussed earlier, the P-wave seismogram is shown. This seismogram is the end product of the simulation done by discretizing the model into 12,700 elements and using 0.05 ms as the sampling rate for the time integration. The same model is then subdivided into 20,500 elements and time integration is done at 0.05 ms sampling rate. The resulting zero-offset P-wave seismogram is presented in Fig. 3a. The reflection event appearing between 300 ms and

500 ms does not show any major change in its attributes as compared to that in Fig. 2a. Next, the physical model of Fig. 2b is discretized into 32,250 elements and time integration is carried out at 0.025 ms time step. The P-wave seismogram for this case is shown in Fig. 3b. Except for the consistent superimposition of a high frequency spiky signal over the actual seismic events, there is hardly any change in the characteristic pattern of the reflection event. In all three P-wave seismograms of Figs. 2a, 3a and 3b, there is neither any variation in the reflection arrival times nor any lateral shift in the amplitudes.

From the above model studies and the detailed analysis performed, the following observations are made:

(i) The Legendre Polynomial Condensation simulation converges both in space and time.

(ii) Ten Legendre Polynomials can accurately preserve the more complex and higher order deformation harmonics of the real earth.

(iii) The results obtained by the direct Finite Element Method (FEM) and Legendre Polyomial Condensation (LPCM) are highly comparable, as depicted in the Table .

CONCLUSIONS

The normal incidence seismograms and the shot profile presented in the previous section indicate that numerical solution for various subsurface structures can be obtained by using the Finite Element Legendre Polynomial Condensation Technique. This method needs small memory and is fast in computing synthetic seismograms. The algorithm also includes automatic mesh generation depending on the anisotropy and heterogeneity in elastic properties in the subsurface. The technique is being used in developing algorithms for the computation of seismograms for three-dimensional structures.

Acknowledgements. Computation were carried out on an HP-9000/330 system at the Department of Geology and Geophysics, I.I.T. Kharagpur, India.

REFERENCES

Asten M.W., Drake L.A and Edwards S.; 1984: *Seismic Love Wave scattering modelled by the finite element method.* Geophysical Prospecting, **32**, 649-661.

Bathe K.J. and Wilson E.L.; 1976: *Numerical Methods in Finite Element analysis.* Printice Hall, Englewood Cliffs, U.S.A.

Bolt B.A. and Smith W.D.; 1976: *Finite element computation of seismic anomalies for bodies of arbitrary shape.* Geophysics, **41**, 145-150.

Choate W.D.; 1982: *A fast algorithm for normal incidence seismograms.* Geophysics, **47**, 196-202.

Cook R.D.; 1974: *Concepts and Application of Finite Element Analysis.* John Wiely and Sons Inc., New York.

Desai C.S. and Abel J.F.; 1972: *Introduction to the Finite Element Method - a numerical method for engineering analysis.* Litton Educational Publishing, New York.

Drake L.A.; 1972: *Love and Rayleigh waves in the horizontally layered media.* Bull. of Seismol. Soc. Am., **62**, 1241-1258.

Drake L.A. and Asten M.W.; 1982: *Wave propagation in irregular coal seams: Finite Element Methods in Engineering.* In: Hoadley P.J. and Stevens L.K. (eds.), Proceedings of the Fourth International Conference in Australia on Finite Element Methods, Dept. of Civil Eng. University of Melbourne, Parkville, Victoria.

Gazdag J.; 1981: *Modelling of acoustic wave equation by transform methods.* Geophysics, **46**, 854-859.

Hilterman F.J.; 1970: *Three dimensional seismic modelling.* Geophysics, **35**, 1020-1037.

Hilterman F.J.; 1982: *Interpretative lessons from Three Dimensional Modelling.* Geophysics, **47**, 784-808.

Kelamis P. and Kjartansson E.; 1985: *Forward modelling in frequency space domain.* Geophysical Prospecting, **33**, 252-262.

Kelly K.R., Ward R.W., Treitel W. and Alford R.M.; 1976: *Synthetic seismograms, a finite difference approach.* Geophysics, **41**, 2-27.

Kosloff D. and Baysal E.; 1982: *Forward modelling by Fourier method.* Geophysics, **47**, 1402-1412.

Lysmer J. and Drake L.A.; 1972: *A finite element method for seismology.* In: Bolt B.A. (ed.), Methods of Computational Physics, Academic Press, London, Vol. 11, pp. 181-286.

Majumdar S. and Samanta A.N.; 1988: *Kinematic Condensation for large slender structures.* 3rd International Conference in Computing in Civil Engineering, Vancouver.

Marfurt K.J.; 1984: *Accuracy of Finite Difference and Finite Element Modelling of the scalar and elastic wave equations.* Geophysics, **49**, 533-549.

Nath S.K., Majumdar S. and Sengupta S.; 1990: *Simulation of seismic responses by Finite Element Consensation.* Presented at the 35th Congress of Indian Society of Theoretical and Applied Mechanics.

Nath S.K., Majumdar S. and Sengupta S.; 1991: *Synthetic seismograms by Finite Element Condensation technique for two dimensional geological structures.* Journal of Association of Exploration Geophysicists, **12**, 45-54.

Nath S.K., Majumdar S. and Sengupta S.; 1991: *Finite element condensation technique in modelling normal incidence synthetic seisimograms.* Indian Journal of Geology, **63**, 6-16.

Reshef M. and Kosloff D.; 1985: *Applications of elastic forward modelling to seismic interpretation.* Geophysics, **50**, 1266-1272.

Reshef M., Kosloff D., Edwards M. and Hsiung C.; 1988: *Three dimensional acoustic modelling by the Fourier method.* Geophysics. **53**, 1184-1193.

Robinson E.A. and Treitel S.; 1966: *Seismic propagation in layered media in terms of communication theory.* Geophysics, **31**, 17-32.

Robinson E.A. and Treitel S.; 1977: *The spectral function of layered system and the determination of the waveforms at depth.* Geophysical Prospecting, **25**, 434-459.

Sherwood J.W.C., Hilterman F.J., Neale R.N. and Chen K.C.; 1983: *Synthetic seismograms with offset for a layered elastic medium.* Offshore Technology Conference, Paper 4508.

Smith W.D.; 1974: *A non reflecting plane boundary in wave propagation problems.* Journal of Computational Physics, **15**, 492-503.

Zienkiewicz O.C.; 1977: *The Finite Element Method.* McGraw-Hill, London.